



Capturing the Current-Overpotential Nonlinearity of Lithium-Ion Batteries by Nonlinear Electrochemical Impedance Spectroscopy (NLEIS) in Charge and Discharge Direction

Sabine Ernst^{1,2}, Tom Patrick Heins^{1,2}, Nicolas Schlüter^{1,2} and Uwe Schröder^{1,2*}

¹ Institute of Environmental and Sustainable Chemistry, Technische Universität Braunschweig, Brunswick, Germany, ² Battery LabFactory Braunschweig, Technische Universität Braunschweig, Brunswick, Germany

OPEN ACCESS

Edited by:

Jun Yan,
Harbin Engineering University, China

Reviewed by:

Shichun Mu,
Wuhan University of
Technology, China
Burak Ulgut,
Bilkent University, Turkey

*Correspondence:

Uwe Schröder
uwe.schroeder@tu-braunschweig.de

Specialty section:

This article was submitted to
Electrochemical Energy Conversion
and Storage,
a section of the journal
Frontiers in Energy Research

Received: 03 June 2019

Accepted: 06 December 2019

Published: 20 December 2019

Citation:

Ernst S, Heins TP, Schlüter N and
Schröder U (2019) Capturing the
Current-Overpotential Nonlinearity of
Lithium-Ion Batteries by Nonlinear
Electrochemical Impedance
Spectroscopy (NLEIS) in Charge and
Discharge Direction.
Front. Energy Res. 7:151.
doi: 10.3389/fenrg.2019.00151

In this paper, a Nonlinear Electrochemical Impedance Spectroscopy (NLEIS) method is presented that allows capturing the nonlinearity of current and overpotential of a lithium-ion battery individually in charge and discharge direction. A DC bias is applied to the battery to shift its operating point to the nonlinear region of current and overpotential. An alternating current of a low amplitude (AC) is simultaneously superimposed in order to investigate the system additionally in the time domain. NLEIS cell spectra and selected electrode-resolved NLEIS spectra are recorded as a function of state of charge and temperature. Furthermore, Distribution of Relaxation Times (DRT) plots obtained from EIS measurements provide information, which electrochemical processes correlate with the occurrence of nonlinear distortions of current and overpotential. Moreover, the occurrence of overpotentials and their degree of nonlinearity at cathode and anode as a function of the state of charge are determined by current pulse measurements.

Keywords: lithium-ion battery, nonlinear electrochemical impedance spectroscopy, overpotential, current-overpotential characteristic, harmonic distortion

INTRODUCTION

Lithium-ion batteries in their entirety represent complex electrochemical systems. Their complexity is mainly reflected in the multitude of characteristically different electrochemical processes taking place within the battery. These processes are responsible for the occurrence of cell overpotentials leading to energy efficiency losses. In order to characterize these electrochemical processes, sophisticated analytical techniques are required. Electrochemical Impedance Spectroscopy (EIS) has proven to be a powerful tool for the characterization of complex electrochemical systems such as lithium-ion batteries (Aurbach, 2000; Atebamba et al., 2010; Illig et al., 2012; Cañas et al., 2013; Heins et al., 2017). The application of this technique allows the differentiation and quantification of major loss processes, making EIS a most powerful electroanalytical tool. Nevertheless, EIS possesses one major limitation: it is restricted to the application of sufficiently small excitations to obey the requirement of linearity between current and voltage. The application of larger input signals results in a distortion of the output signal, compromising the measurement. Moreover, within the EIS, only the mean impedance of charge and discharge direction, i.e., the impedance around the origin of the current-voltage ratio, is determined. Conventional EIS is therefore not capable:

- (1) to reflect the nonlinear character of electrode kinetics.
- (2) to determine the impedance in charge and discharge direction individually.

Therefore, in this work, an approach to Nonlinear Electrochemical Impedance Spectroscopy (NLEIS) will be presented to investigate the nonlinear current-voltage ratio of lithium-ion batteries in charge and discharge direction individually. Moreover, we examined overpotentials occurring at the cathode and anode in charge and discharge direction.

THEORY

Overpotentials in Lithium-Ion Batteries

Whenever a current is being applied to an electrochemical system (e.g., lithium-ion batteries), its open cell voltage (OCV—the equilibrium voltage) is altered by the cell overpotential η . The magnitude of the overall overpotential is determined by several processes—the ohmic overpotential (caused by ionic conductivity of the electrolyte, electronic conductivity of the electroactive material, and the electronic conductivity of the current collector), the contact resistance (caused by the resistance between electroactive material and current collector) the charge transfer overpotential (caused by activation energy at the electrode surfaces) and the diffusion overpotential (caused by lithium ion diffusion especially near the electrode surfaces and the solid-state diffusion inside the active electrode material) (Vetter et al., 2005; Jossen, 2006).

$$\eta = \eta_{\text{ohmic}} + \eta_{\text{contact}} + \eta_{\text{diff}} + \eta_{\text{ct}} \quad (1)$$

Provided that the OCV of an electrochemical cell remains constant over an entire measurement period, the relation of current and voltage is exclusively determined by the magnitude of overpotential (η -characteristic). For low currents, the $I\eta$ -relation remains almost linear, whereas for moderate and higher currents it develops into a nonlinear behavior. The individual overpotentials depicted in Equation (1) have different impacts on nonlinear distortion. Thus, the ohmic and the contact overpotentials cause linear $I\eta$ -characteristics. Charge transfer and diffusion transfer processes on the other hand result in nonlinear $I\eta$ -behavior (Bard and Faulkner, 2001). **Figure 1** illustrates the major overpotentials responsible for the nonlinear distortion of current and overpotential within a lithium-ion battery for the example of the discharge direction. The cathodic charge transfer overpotential (η_{ct}) involves the stripping of the solvation shell followed by the phase-transfer into the active electrode material (intercalation). The anodic intercalation process differs: lithium-ions first pass through the solid electrolyte interphase (SEI) and subsequently intercalate into the active material (Xu et al., 2010). For the sake of simplicity, however, we do not consider this difference in the following discussions.

The charge transfer overpotential is one of the decisive parameters in electrochemical kinetics as it reflects the resistance to the electrode surface reaction. It is mathematically linked to the current density by Butler-Volmer Equation (Equation 2),

providing that mass-transfer effects are not considered (Bard and Faulkner, 2001; Jossen, 2006).

$$i = i_0 \left[e^{\frac{\alpha F \eta}{RT}} - e^{-\frac{(1-\alpha) F \eta}{RT}} \right] \quad (2)$$

Here, i and i_0 represent current density and exchange current density, respectively. Since Butler-Volmer considers that electrode reactions (charge transfer) may be asymmetric, a transfer coefficient (α) describes the proportion of forward and backward reaction at the corresponding electrode (Bard and Faulkner, 2001).

Generally, diffusion processes take place as response to a concentration gradient. Therefore, they occur in the bulk solution particularly near the electrode surface due to the reaction of the electroactive species ($\eta_{\text{diff,liq}}$) (Bard and Faulkner, 2001). After intercalating into the active material, the lithium ions diffuse toward free lattice sites in the cathode material (in case of charging the same process takes place at the anode). This represents the solid-state diffusion process ($\eta_{\text{diff,solid}}$) (Jossen, 2006).

In this work, we focused on the investigation of electrochemical processes causing nonlinear distortion of current and overpotential such as charge transfer and diffusion processes (**Figure 1**). We present an approach to NLEIS where the operating point of the lithium-ion battery on the $I\eta$ -curve is shifted by a DC bias to the nonlinear region of current and overpotential. We are therefore able to consider the nonlinearity of charge and discharge direction individually. An alternating current of a small amplitude is simultaneously superimposed to investigate the system in the time domain.

Nonlinear Characteristics of Lithium-Ion Batteries

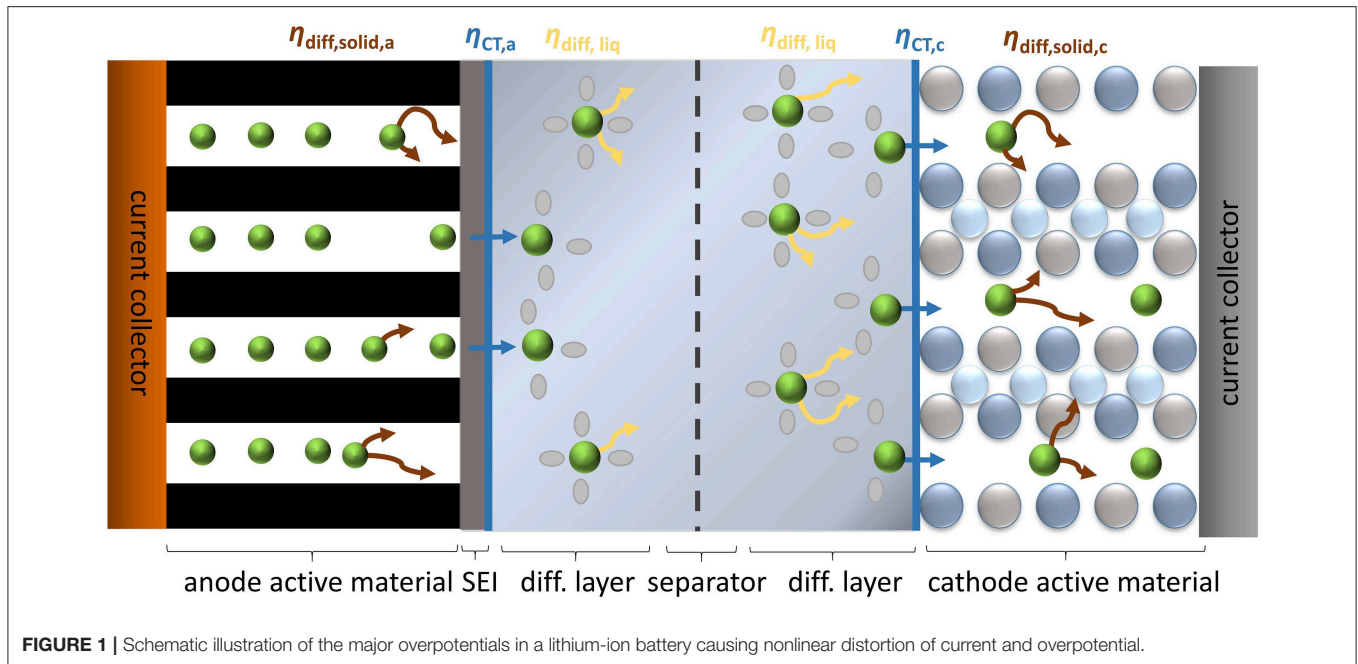
In mathematical terms, nonlinear relation of current and overpotential means the absence of the strict validity of Ohm's law. This implies that results of conventional EIS, which requires the validity of Ohm's law, can be compared to results of nonlinear measurements only to a limited extent. In spectral analytics, nonlinearity appears in higher harmonics ($H_{x>1}$) of the output signal, representing integer multiples of the frequency of the input signal (H_1). The general distortion of a signal can be expressed by Total Harmonic Distortion (THD) (Shmilovitz, 2005).

$$THD = \frac{\sqrt{\sum_{x=2}^n (H_x)^2}}{H_1} \quad (3)$$

$$\text{Where } H_x \{x \in \mathbb{Z}^+ | x > 1\}$$

In this study, however, the occurrence of each higher harmonic is considered individually to investigate its characteristic response and therefore Equation (4) was utilized. Each higher harmonic is normalized to the fundamental frequency (H_1). The result gives the magnitude of the corresponding higher harmonic (H_x).

$$\text{magnitude}(H_x) = \frac{\sqrt{(H_x)^2}}{H_1} \quad (4)$$



MEASUREMENT METHODS

Current Pulse Measurement

The current pulse measurements were used to determine the characteristics between current and overpotential.

A current pulse of 1/5 C with a duration of 10 s is applied to the lithium-ion battery, followed by a relaxation step of 5 min. The procedure is subsequently repeated for a negative current pulse (**Figure 2**) in order to avoid time deviations of the system due to a change of the state of charge. The height of the current pulse is then increased to a certain value (see Experimental section). The current pulse duration was chosen according to the smallest time constant of the system (determined by EIS), to ensure that all electrochemical processes are captured.

After each current pulse pair, the value of the OCV was compared to the initial OCV. If this value deviated by more than 2%, the data were discarded to prevent results from being compromised due to a change of the system's state. To determine the overpotentials in charge and discharge direction, the following equations were used:

$$\eta_{charge} = E_{CELL,max} - E_{CELL,OCV} \quad (5)$$

$$\eta_{discharge} = E_{CELL,min} - E_{CELL,OCV} \quad (6)$$

In order to estimate the degree of nonlinearity between current and overpotential, the dimensionless Pearson Correlation Coefficient (r) was utilized (Equation 7) (Ahlgren et al., 2003).

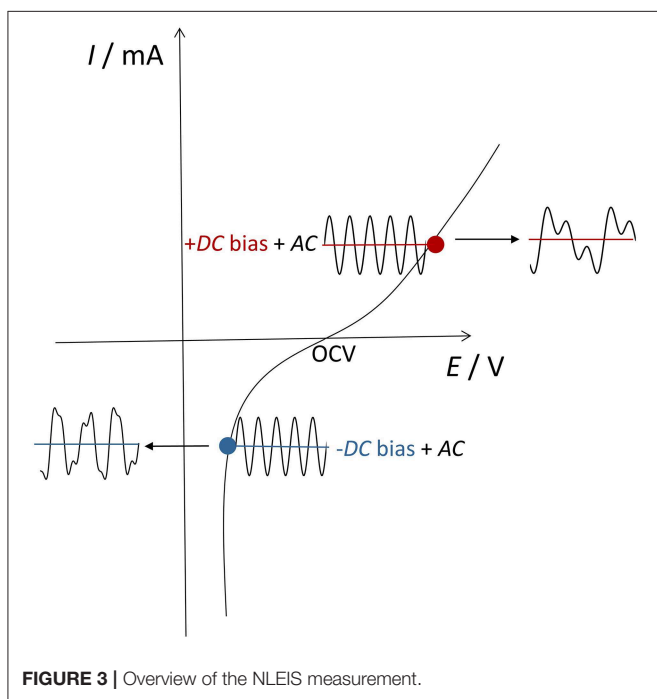
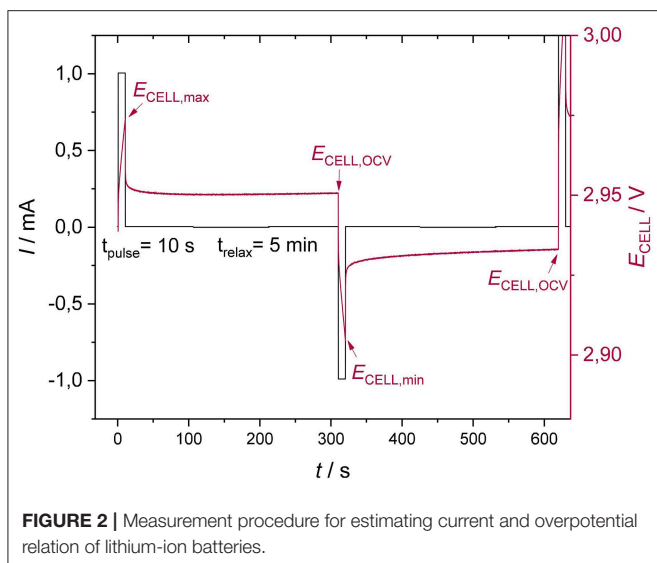
$$r = \frac{\sum_{i=1}^n (I_i - \bar{I})(\eta_i - \bar{\eta})}{\sqrt{\sum_{i=1}^n (I_i - \bar{I})^2 \sum_{i=1}^n (\eta_i - \bar{\eta})^2}} \quad (7)$$

Where $\bar{I} = \frac{1}{n} \sum_{i=1}^n I_i$ and $\bar{\eta} = \frac{1}{n} \sum_{i=1}^n \eta_i$; r takes values between 1 and -1 . At a value of 1 or -1 , there is a complete positive or

negative linear relationship between I and η . For $r = 0$, I , and η are uncorrelated.

NLEIS

To successfully investigate the nonlinearity of an electrochemical system, some fundamental approaches have already been proposed (Kiel et al., 2008; Mao et al., 2010; Harting et al., 2017; Murbach et al., 2018; Zabara et al., 2019). The main similarity between the underlying methods is that the operating point of the electrochemical system on the $I\eta$ -curve is shifted to the range of nonlinearity. In the current work, the operating point of the lithium-ion battery is shifted by applying a sufficiently high direct current (DC). For investigating the system in the time domain, an alternating current (AC) with a small amplitude is simultaneously superimposed. The distorted output signal contains not only the fundamental frequency but also its higher harmonics. By means of Fast Fourier Transform (FFT) its discrete frequency coefficients are isolated from the signal. The fourier coefficients are then normalized to the fundamental frequency and the result is used to estimate the magnitude of each higher harmonic. The NLEIS spectra are recorded with alternating current pulses—according to measurement procedure of the I -pulse measurements. First, a positive direct current is applied and an additional alternating current of a specific frequency is superimposed. Subsequently, the corresponding negative direct current with the alternating current of the same frequency is measured (**Figure 3**). The main advantage of this method is that we can determine nonlinearity in charge and discharge direction individually. Note, that we are windowing our digitized signal to prevent aliasing. Therefore, the higher harmonics will be suppressed to a certain extent due to this drift correction.



Generally, the underlying approach (**Figure 3**) is widely used for investigating the harmonic characteristics of highly nonlinear electronic components such as diodes (Suematsu et al., 1982; Caverly and Hiller, 1987; Way, 1987). In terms of electrochemical systems there are several methods performing DC and AC experiments in a single measurement [e.g., Dynamic-EIS (Sacci et al., 2014; Zhang et al., 2014; Huang et al., 2015)] but without considering the system's nonlinearity. There are only a few publications, however, of DC/AC experiments that are used to specifically investigate nonlinearity of electrochemical systems (Xu and Riley, 2013). To the best of our knowledge, this measurement technique has not been applied to energy storage

media such as lithium-ion batteries, yet. Since we apply a DC bias, occurring higher harmonics can be the result of a system's potential drift or capacitances. Therefore, we also performed an experiment with a supercapacitor that has a capacitance similar to our system (ca. 22 mF). If potential issues like voltage drift or capacitances generally cause the appearance of higher harmonics, they have to become visible in this experiment. Since we did not see significant higher harmonics (<0.1%) (see **Supplementary Material**), these issues can be excluded as source for higher harmonics in case of our measurement setup.

For a more detailed understanding of the measurement method and its development for lithium-ion batteries in general refer to the **Supplementary Material**.

EIS

EIS measurements were performed in order to correlate the tendency of overpotentials with data obtained from EIS. Additionally, EIS spectra were utilized to determine which electrochemical processes of the lithium-ion battery are attributed to the frequency range captured in the NLEIS measurements. Therefore, the time constants obtained using DRT (Saccoccio et al., 2014; Wan et al., 2015) are compared to the occurrence of higher harmonics from the NLEIS spectra.

RESULTS

In order to gain a deeper understanding of when nonlinearity in the studied lithium-ion batteries becomes relevant and whether the electrode reactions are asymmetric, we initially recorded $I\eta$ -curves by current-pulse measurements (I -Pulse). The $I\eta$ -curves were recorded up to a current pulse of 34 mA ($\sim 7C$). This current limit was chosen in order to avoid irreversible degradation of electrochemical functionality by reaching certain potentials. We therefore chose in this case a cell voltage of 3.3 V to ensure that e.g., the anode's potential does not drop below 0 V preventing metallic lithium deposition on the anode surface even at high current densities (Bugga and Smart, 2010).

In the following figures, all data referring to the charge direction are shown in red and the results of the discharge direction are represented in blue.

The $I\eta$ -curves for anode and cathode indicate asymmetric kinetics of the electrode reactions with respect to charge and discharge direction, with the asymmetry being considerably more pronounced at the cathode (**Figure 4**). The cathode's $I\eta$ -curve in discharge direction indicates much higher overpotentials than in charge direction. It is therefore necessary to consider the positive and negative current range individually to obtain differentiated information about the kinetics of the electrode reactions in charge and discharge direction.

Obviously, it is not possible to apply such a high DC bias, 34 mA, to record NLEIS, because the change of the cell properties due to a shift in the state of charge (over time) would be significant. In order to avoid large time deviations of the system, therefore, an operating point on the $I\eta$ -curve was selected, which already points to nonlinearity between current and overpotential, for which, however the lowest possible current is required.

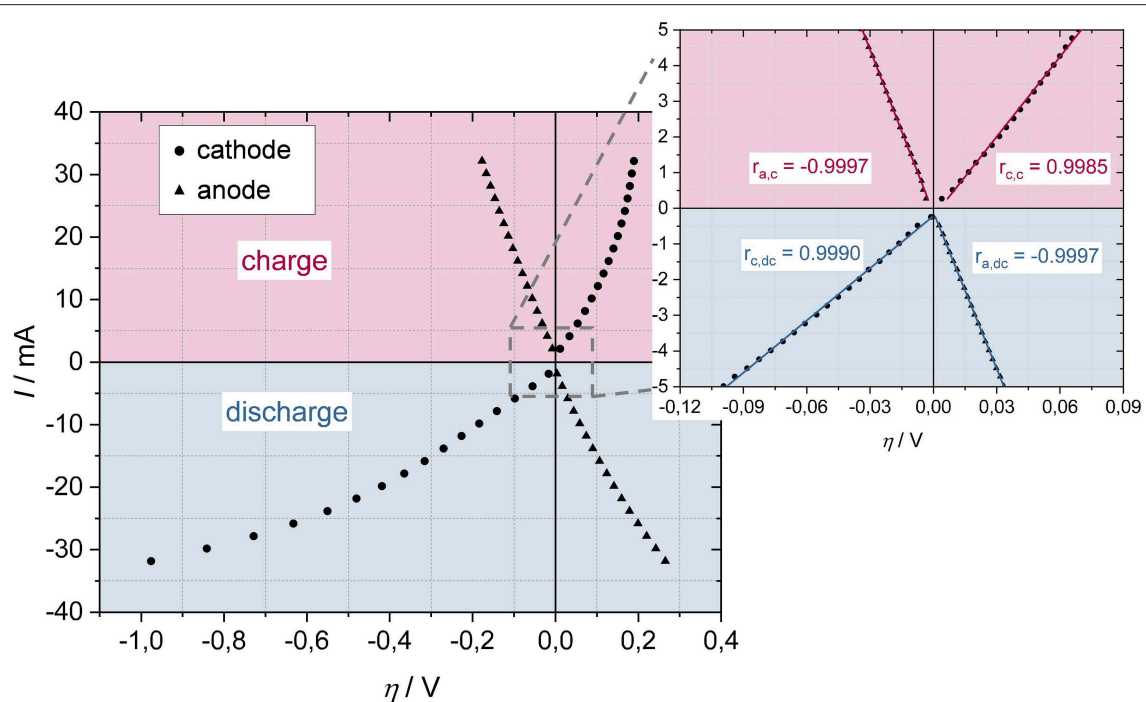


FIGURE 4 | $|I\eta|$ characteristic of the investigated lithium-ion battery ($\Delta I = 2$ mA) (**Left**) with the corresponding correlation coefficients for a DC bias of max. 5 mA ($\Delta I = 0.5$ mA) (**Right**) of anode (r_a) and cathode (r_c) in charge (red) and discharge (blue) direction at a cell voltage of 3.3 V recorded at 20°C.

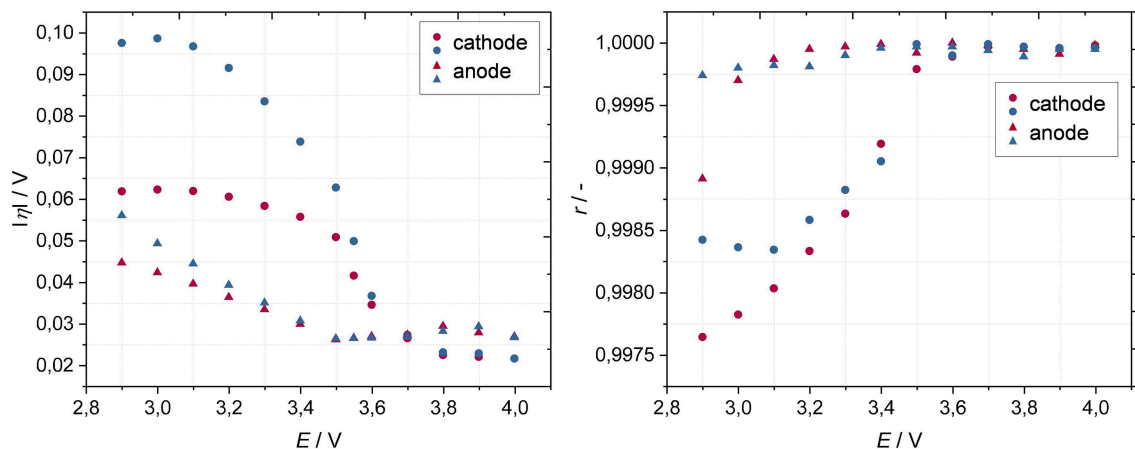
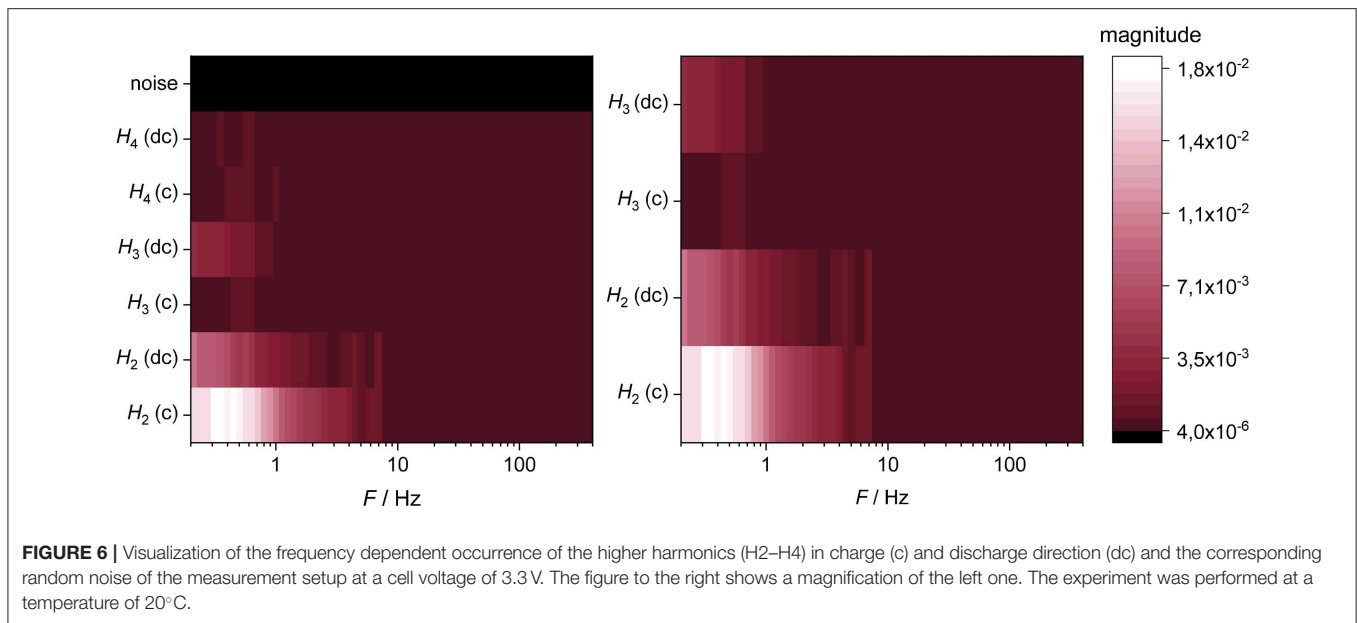


FIGURE 5 | Overpotentials based on a DC bias of 5 mA (**Left**) and corresponding correlation coefficients based on a DC bias range of 1–5 mA ($\Delta I = 1$ mA) (**Right**) of cathode and anode in charge (red) and discharge (blue) direction as a function of cell voltage at a temperature of 20°C.

The magnified figure to the right (**Figure 4**) shows the range selected to measure NLEIS with corresponding r . Accordingly, the following NLEIS spectra were recorded with 5 mA DC (ca. 1 C) and 2 mA AC. Previous to this study we analyzed different DC bias (2, 5, 7, and 9 mA) to investigate how the DC bias affects the higher harmonics. We found out that the values of the higher harmonics increase with increasing DC bias, but the course of the harmonic values remains the same (same in quality). At a value of 9 mA the harmonics decrease, probably

due to a significant change in the cell voltage. Therefore, we chose a DC bias of 5 mA, since the higher harmonic values' signal to noise ratio is satisfactory and the change in the cell voltage is less. Further, we chose 2 mA AC since the impedance spectra are performed with that amplitude. We therefore ensure, that our lithium-ion battery system does not become nonlinear due of the AC signal, but only because of the applied DC bias. Additionally, the signal to noise ratio is satisfactory for this amplitude.



State of Charge

Current Pulse Results

All following current pulse measurements were evaluated at a DC bias of 5 mA, according to the DC bias of recorded NLEIS spectra.

The overpotentials of the cathode are strongly dependent on the state of charge of the lithium-ion battery and generally increase with decreasing cell voltage (**Figure 5**). According to literature, this can be explained by an increase of the charge transfer resistance (Wu et al., 2005). In addition, inhibited solid-state lithium ion diffusion within NMC ($\text{LiNi}_{1/3}\text{Co}_{1/3}\text{Mn}_{1/3}\text{O}_2$) is responsible for higher overpotentials at lower state of charges. This phenomenon is due to a contraction of a certain crystal plane within NMC at high lithiation degrees (Wiemers-Meyer et al., 2016). Further lithium intercalation requires large negative potentials, which leads to significant overpotentials in discharge direction (Latz and Zausch, 2013). Oppositely, during charging (decrease of lithiation degree), the solid-state lithium-ion diffusion becomes facilitated due to an expansion of the crystal plane. The lithium-ion mobility becomes thereby largest at 50% state of charge (Wiemers-Meyer et al., 2016). Moreover, the electronic conductivity of NMC increases with delithiation, which is attributed to the presence of mixed $\text{Ni}^{3+}/\text{Ni}^{4+}$ valence states, therefore contributing to a reduction of overpotentials with increasing state of charge (Amin and Chiang, 2016). At lower state of charges (at 3.3 V and below) the overpotentials are much higher for the discharge direction than for the charge direction. This effect is significantly enhanced at higher current values (**Figure 4**). Moreover, the nonlinear relation between current and overpotential (**Figure 5**, right) increases especially at the cathode with decreasing state of charge which corresponds to the tendency of overpotentials (**Figure 5**, left). The anode's overpotentials, in contrast, are only slightly affected by the state of charge of the lithium-ion battery. The values of its overpotentials

are about half the cathode's overall overpotential. The anode is therefore significantly less kinetically inhibited. The slightly increasing overpotential in lower state of charge range might be due to an increase of the charge transfer resistance and the lower electronic conductivity of delithiated graphite (Umeda et al., 2001; Park et al., 2010; Gordon et al., 2017). In contrast to the cathode, the lithium solid-state diffusion within the graphite makes only a small contribution to the overpotentials, since the diffusion coefficient only weakly depends on the state of charge and is generally slightly larger than the diffusion coefficient of lithium within NMC (Yu et al., 1999; Wu et al., 2012). At a cell voltage of 3.7 V and above the overall overpotentials for anode and cathode become insignificantly small in both charge and discharge direction. In order to exemplarily correlate the tendency of overpotentials with EIS data, electrode-resolved EIS spectra in dependence of the state of charge are depicted in the **Supplementary Material**. In this work we primarily focus on the qualitatively correlation.

NLEIS

Initially, we investigated the nonlinearity for a cell voltage of 3.3 V to determine, which higher harmonics of relevant magnitude generally occur.

Figure 6 indicates that the magnitude of harmonics decreases from the 2nd harmonic to higher harmonic orders and is generally higher in charge direction. The 2nd harmonic clearly appears in the middle and lower frequency range, whereas the 3rd harmonic is only slightly visible in the low frequency range of the discharge direction. In contrast, the 4th harmonic does not exhibit any relevant values. Based on this result, in further investigations only the 2nd and 3rd harmonics are considered. The random noises of the 2nd and 3rd harmonic are quantified by an ohmic resistance of 10 Ω .

NLEIS cell spectra were recorded at four different cell voltages: 2.9, 3.3, 3.7, and 4.0 V (**Figure 7**).

In general, the 2nd harmonic is negligible at a cell voltage of 3.7 V and above, but increases with decreasing voltage (**Figure 7**). This correlates with the described tendency of the overpotentials' charge-dependencies. At lower cell voltages, the 2nd harmonic occurs at frequencies below ~ 4 Hz and increases in its magnitude with decreasing frequency. Furthermore, the 2nd harmonic is significantly more pronounced in charge direction than in discharge direction, which agrees with the correlation coefficients (**Figure 5**, right), but is contrary to the overpotentials being higher in discharge direction. Interestingly, the magnitude of 2nd harmonic does not change significantly between 2.9 and 3.3 V, especially in charge direction. The 3rd harmonic occurs only in discharge direction at lower cell voltages from a frequency of 0.7 Hz (**Figure 7**) in relevant orders of magnitude.

To gain a deeper understanding which electrode—cathode or anode—causes the main nonlinearity, electrode-resolved NLEIS spectra at a cell voltage of 3.3 V were recorded (**Figure 8**, top). Therefore, the excitation signal was applied to the cell and the signals of anode and cathode were recorded individually using an integrated reference electrode. In addition, an electrode-resolved DRT plot (**Figure 8**, bottom) is shown to compare which processes take place in the corresponding frequency range according to EIS at this cell voltage. The corresponding impedance spectra are found in the **Supplementary Material**.

According to the upper part of **Figure 8**, nonlinearity occurs especially at the cathode at frequencies below 4 Hz, with the nonlinearity in charge direction being much more pronounced than in discharge direction. According to the DRT-plot (**Figure 8**, bottom), the frequency range below 8 Hz is associated with the charge transfer resistance of the cathode and agrees with the appearance of the 2nd harmonic at the cathode. The 2nd harmonic of the anode is negligible over the entire frequency range, which is possibly a result of the charge transfer resistance being very low. We can therefore assume that the appearance of the 2nd harmonic correlates with the presence of a kinetic reaction inhibition. The magnification exhibits that even the magnitude of 3rd harmonic of the cathode (at a frequency below 0.7 Hz) is greater than the 2nd harmonic of the anode.

Interestingly, the cathode's higher overpotentials in discharge direction (**Figure 5**, left) are not reflected by NLEIS in form of the 2nd harmonic (higher in charge direction) (**Figure 8**). Therefore, the higher overpotentials in discharge direction may be expressed in form of the 3rd harmonic. Possibly, the inhibited solid-state lithium-ion diffusion within NMC due to the high degree of lithiation causes the occurrence of the 3rd harmonic. The fact that the 3rd harmonic becomes only visible at lower state of charges in the lower frequency range supports the assumption. Moreover, the occurrence of the 3rd harmonic in response to diffusion processes has already been suggested in literature (Wolff et al., 2018, 2019).

Temperature

Current Pulse Results

The following temperature dependent $I\eta$ -characteristics are based on a DC bias of 5 mA. In this case a constant cell

voltage of 3.7 V was chosen (instead of 3.3 V depicted in **Figure 6**). Since the nonlinearities at cell voltages of 3.7 V and at a temperature of 20°C are negligible (**Figures 5, 7**), we can be sure that the occurrence of higher harmonics at 3.7 V ($T < 20^\circ\text{C}$) is exclusively due to a slower kinetic as a result of temperature reduction.

As expected, the overpotentials of both, cathode and anode, are strongly dependent on temperature and increase with decreasing temperature (**Figure 9**, left), with the overpotentials being higher in discharge direction. With decreasing temperature, the asymmetry of overpotentials of charge and discharge direction becomes more pronounced, especially at the cathode. The tendency of the correlation coefficients coincides with the tendency of the overpotentials and exhibit a predominantly higher degree of nonlinearity at the cathode in charge direction. In order to correlate the tendency of overpotentials with data obtained from EIS, electrode-resolved EIS spectra in dependence of the temperature are found in the **Supplementary Material**.

NLEIS

Initially, we recorded a NLEIS cell spectrum at 0°C (and at a cell voltage of 3.7 V), to investigate, which harmonics occur at lowered temperature.

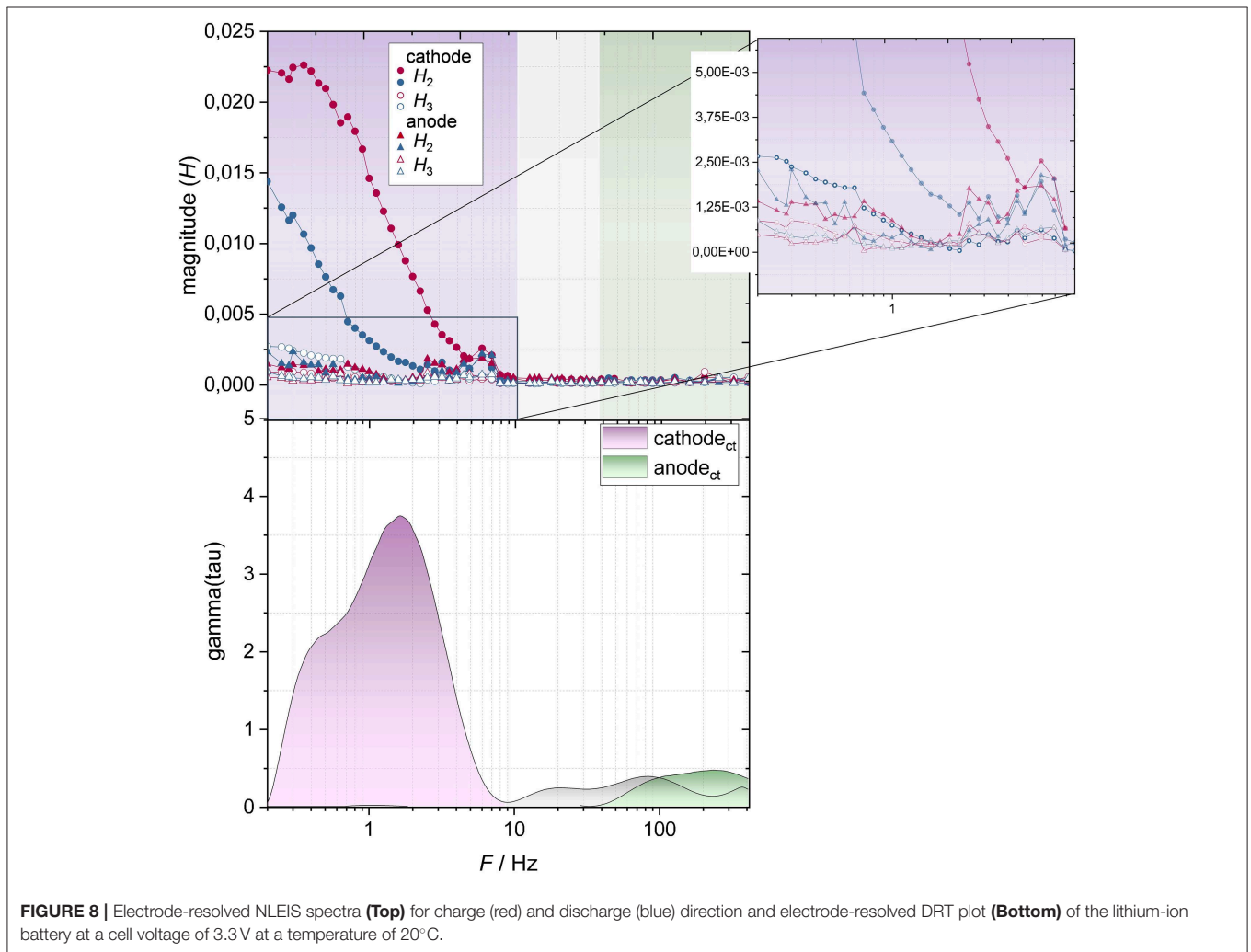
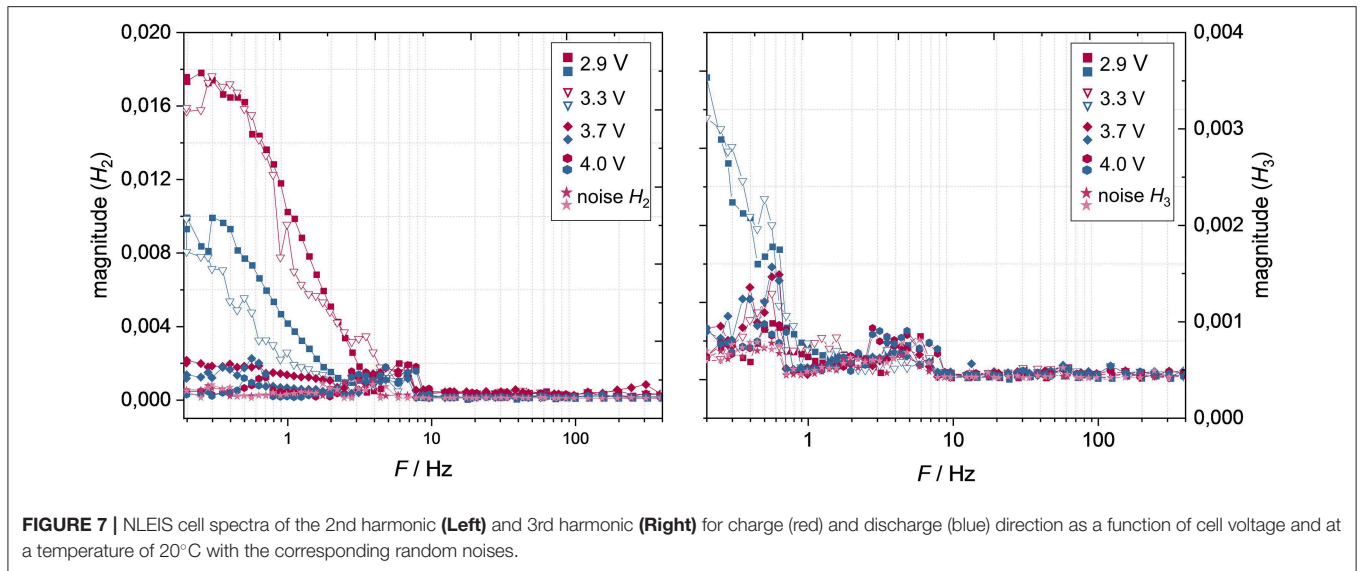
At a cell voltage of 3.7 V and a temperature of 0°C only the 2nd harmonic appears. The 3rd and 4th harmonic are negligible in charge and discharge direction.

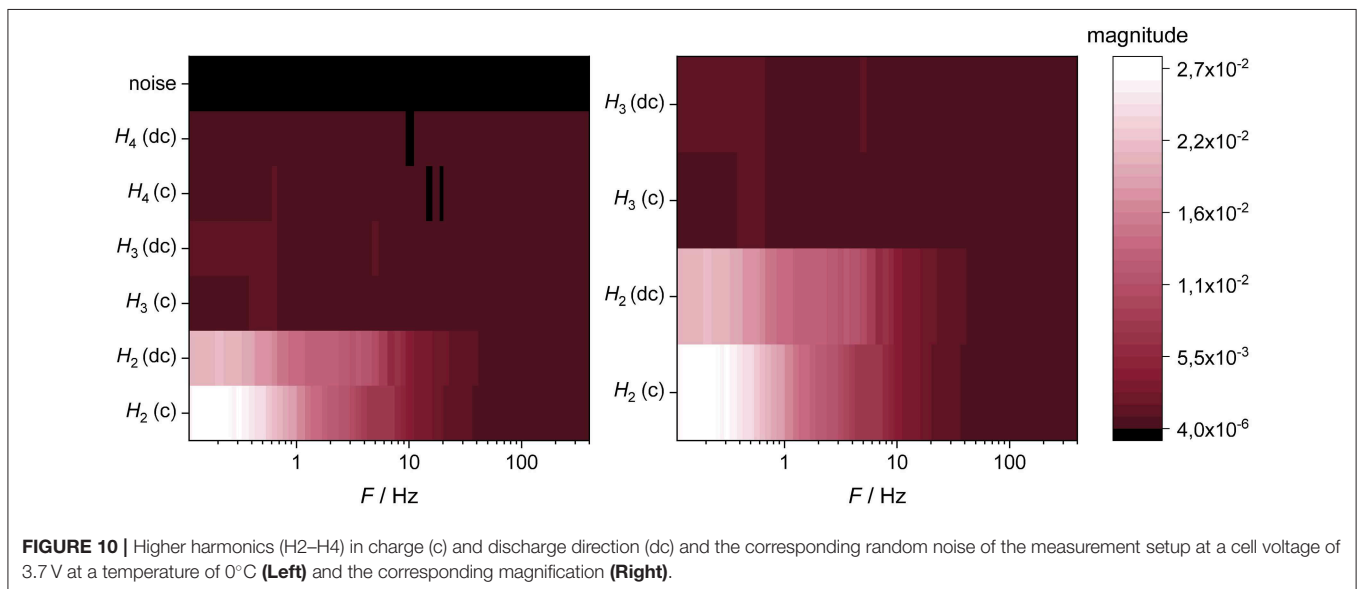
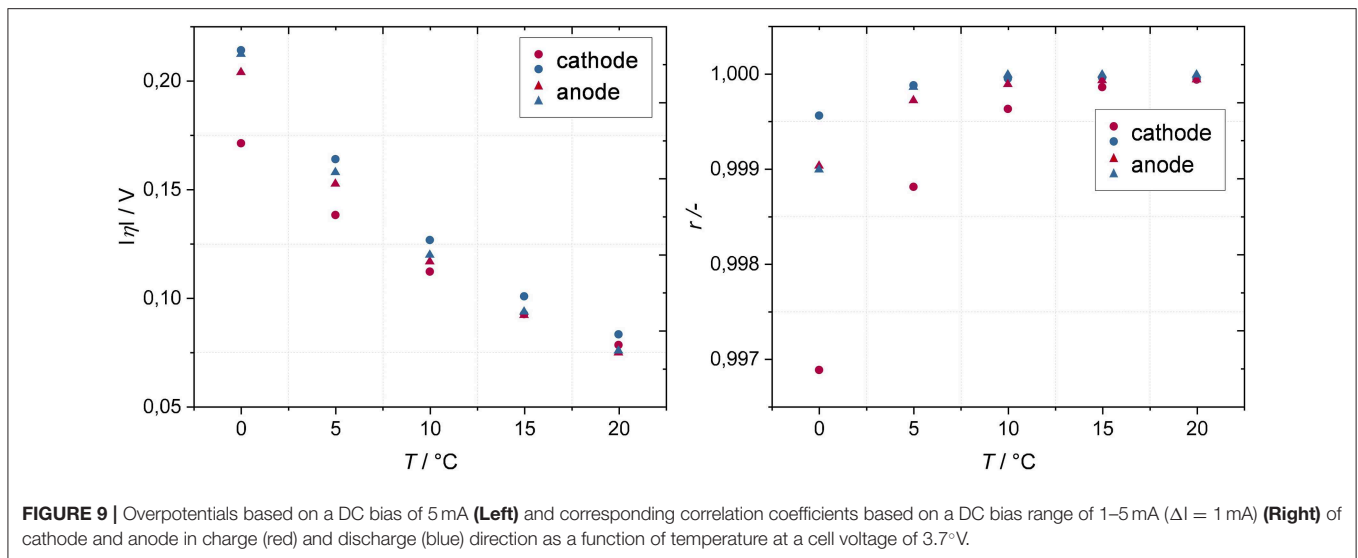
In the following measurements, the occurrence of nonlinearities as a function of temperature will be investigated. For this purpose, NLEIS spectra are recorded at a cell voltage of 3.7 V in the temperature range from 0 to 20°C. Although the 3rd harmonic exhibits no relevant values in **Figure 10**, it is further considered for the sake of completeness. The random noises of the 2nd and 3rd harmonic are quantified by an ohmic resistance of 10 Ω .

The magnitude of the 2nd harmonic decreases with increasing temperature (**Figure 11**, left), and at a temperature of 15°C and above the 2nd harmonic becomes insignificant. The 2nd harmonic appears at frequencies below ~ 10 Hz and increases with decreasing frequency until it reaches a plateau at ~ 0.4 Hz. Down to 6 Hz, the 2nd harmonic is very similar for charge and discharge direction, whereas in the frequency range of 6–2 Hz the discharge direction becomes predominant. This tendency inverts below 2 Hz, where the 2nd harmonic in charge direction becomes significantly larger than in discharge direction.

At a frequency of 0.9 Hz the 3rd harmonic increases but, however, decreases further at a temperature of 10°C and above (**Figure 11**, right). At a temperature of 5°C and below only a slight increase of the 3rd harmonic can be seen in the lower frequency range. Interestingly, although the magnitude of the 2nd harmonic at 0°C (and a cell voltage of 3.7 V) is greater than the 2nd harmonic at a cell voltage of 2.9 V and a temperature of 20°C (**Figure 7**), the 3rd harmonic does not significantly arise here (**Figures 10, 11**, right). However, since the magnitudes of the 3rd harmonic are so small, further interpretation of these is initially omitted.

An electrode-resolved NLEIS spectrum (**Figure 12**, top) with a corresponding DRT plot (**Figure 12**, bottom) of the lithium





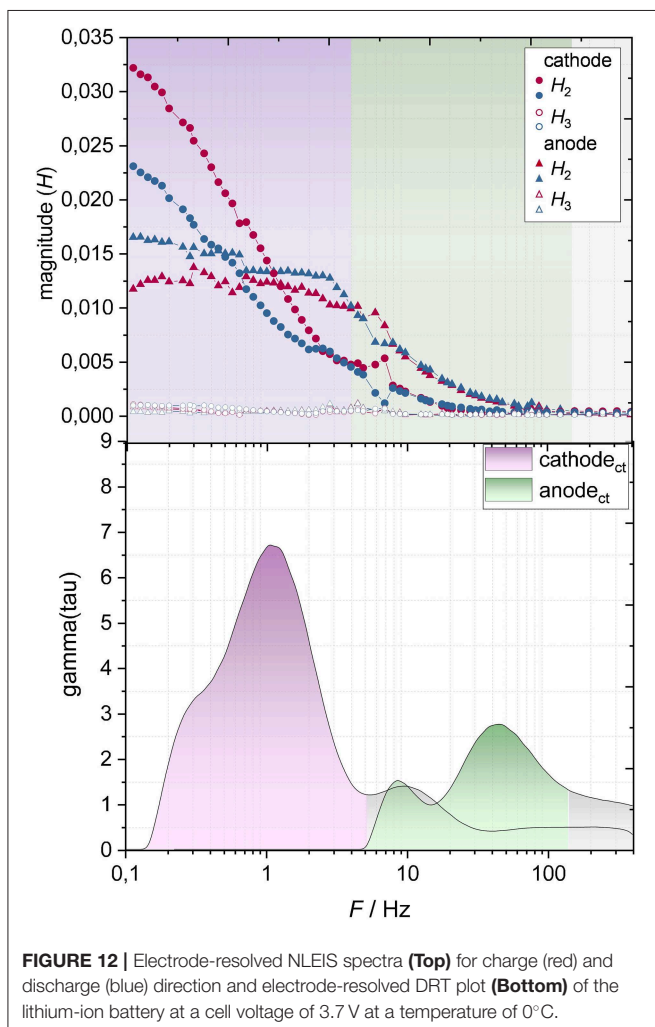
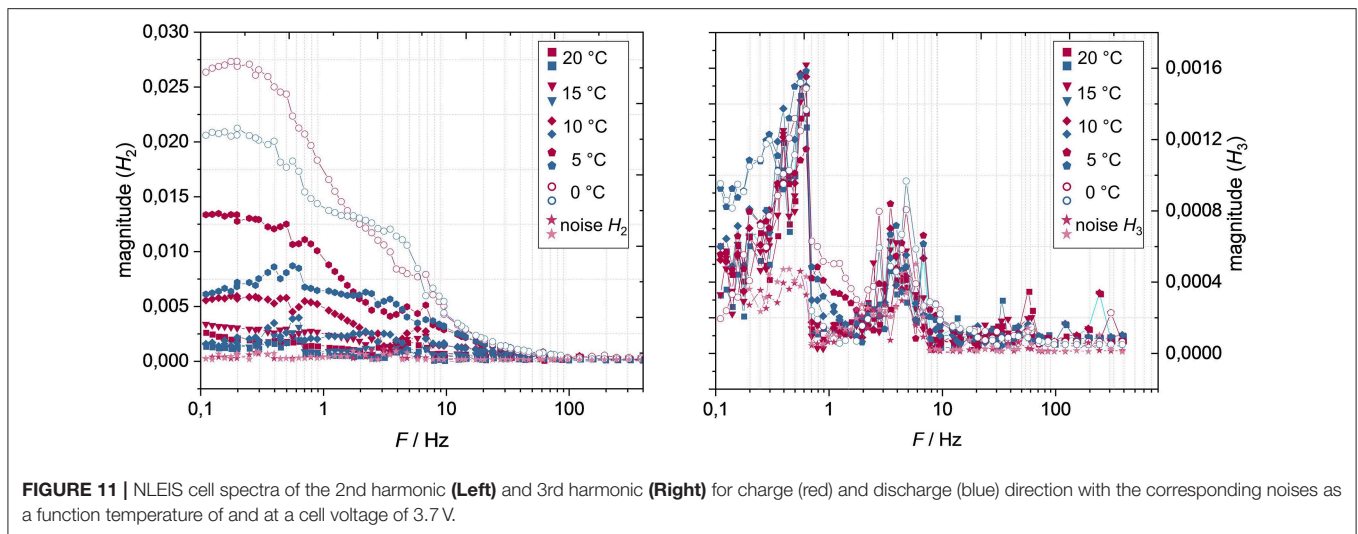
ion-battery at 3.7 V and 0°C are further shown. The according impedance spectra are found in the supporting information.

The 2nd harmonic of the anode arises at frequencies below ca. 60 Hz, whereas the cathode's 2nd harmonic appears not before a frequency of 20 Hz. The frequency range of the anode's 2nd harmonic coincides with its charge transfer resistance (**Figure 12**, bottom). The DRT plot further exhibits that the anodic charge transfer resistance increases relative to the cathodic charge transfer resistance compared to the bottom of **Figure 8**. It can therefore be assumed that, due to the higher charge transfer resistance, in this case a 2nd harmonic arises at the anode.

Lowering the frequency from 20 Hz down to 4 Hz leads to an increase of the 2nd harmonic, after which it reaches a plateau. Before reaching the plateau, the 2nd harmonic of the anode is generally higher than that of the cathode, which is probably due to the lower time constant of the anode's charge transfer resistance. This tendency inverts at a frequency of ca. 1 Hz,

where the 2nd harmonic of the anode remains constant and the cathode's 2nd harmonic increases further. The occurrence of the 2nd harmonic matches, as in the case of the anode, with the time constant of its charge transfer resistance (**Figure 12**, bottom). Furthermore, the charge direction at the cathode depicts much higher nonlinearities than the discharge direction. Since the 2nd harmonics of the anode of charge and discharge direction are very close to each other, no clear directional dependence (charge or discharge) can be found. This result indicates that the kinetics of the anodic electrode reaction is more symmetrical than the electrode reaction at the cathode regarding charge and discharge direction. The 3rd harmonics' magnitude is compared to the 2nd harmonics' magnitude negligible for both electrodes.

The change of the 2nd harmonic in the NLEIS cells spectra (**Figure 11**, left) with respect to charge and discharge direction can be explained with the change of the 2nd harmonics' magnitude between anode and cathode. Additionally,



the plateau in the lower frequency range of cell spectra can be attributed to the anode's contribution. We can therefore assume that the NLEIS cell spectra represent the sum of the

anodic and cathodic nonlinear contributions (in this case the 2nd harmonic).

When comparing the two electrode-resolved spectra (**Figures 8, 12**), it is noticeable that the 2nd harmonic, particularly at the anode, has significantly different courses depending on cell voltage or temperature. While the anode exhibits virtually no nonlinearities at a lower state of charge (3.3 V) (**Figure 8**), its contribution to nonlinearity at lowered temperature (0°C) is comparable to the contribution of the cathode (**Figure 12**). This observation leads us to the assumption that the overpotentials contributing to nonlinearity at varying cell voltages are either qualitatively different from the overpotentials that occur with temperature changes, or the same overpotential causes significantly different distortion of overpotential and current depending on state of charge or temperature changes. On the basis of the experiments carried out, we assume that the 2nd harmonic reflects the kinetic of the charge transfer reaction. Therefore, the same overpotential (charge transfer) shows different expressions in dependence of temperature changes and changes in state of charge. The fact that the 2nd harmonic exhibits a high temperature dependence and a rather low dependence on the state of charge may support the assumption (André et al., 2011; Farmann et al., 2016).

CONCLUSION

In this work, in addition to the investigation of nonlinear distortion of current and overpotential using a new approach to NLEIS, we also examined the state of charge and temperature dependent anodic and cathodic current-overpotential characteristics of a lithium-ion battery. For the first time, this NLEIS method allows to individually address nonlinearity in charge and discharge direction of lithium-ion batteries.

We show that the reaction kinetics at cathode and anode, according to Butler-Volmer, are asymmetric, with the cathodic asymmetry being much more pronounced than the anodic.

The overpotentials of the cathode depend significantly on the state of charge, whereas the respective overpotentials of the

TABLE 1 | Electrode composition of the investigated lithium-ion battery.

Component	Mass fraction	Chemical compound	Manu-facturer
Active material	91 wt.-% (anode)	Graphite (SMG A4)	Hitachi
	90 wt.-% (cathode)	LiNi _{1/3} Co _{1/3} Mn _{1/3} O ₂ (HED NCM-111)	BASF
Binder	5 wt.-% (anode)	Polyvinylidenefluoride (Solef 5130)	Solvay
	4 wt.-% (cathode)		
Conducting agent	2 wt.-%	Graphite (C-Nergy SFG 6L)	Imerys
Conductive carbon black	2 wt.-% (anode)	Carbon black (C-Nergy Super C65)	Imerys
	4 wt.-% (cathode)		

TABLE 2 | Experimental parameters for EIS spectra, I-Pulse measurements, and NLEIS spectra as a function of temperature.

	T	Freq	AC	DC	E _{cell}
EIS	0°C	200 kHz–5 mHz (30 freq. per decade)	2 mA	/	3.7 V
I-Pulse	20–0°C; ΔT = 5°C	/	/	±1–5 mA ΔI = 1 mA	3.7 V
NLEIS (full cell)	20–0°C; ΔT = 5°C	400–0.1 Hz (10 freq. per decade)	2 mA	±5 mA	3.7 V
NLEIS (electrode-resolved)	0°C	400–0.1 Hz (10 freq. per decade)	2 mA	±5 mA	3.7 V

anode only show a slight dependence. In the NLEIS cell spectra, the nonlinearity (2nd harmonic) increases with decreasing SOC, which correlates with the tendency of overpotentials. The electrode-resolved spectra at a cell voltage of 3.3 V clearly show nonlinear distortion (2nd harmonic) at the cathode in the medium and low frequency range, whereas the nonlinear distortion at the anode is negligible.

Moreover, the 3rd harmonic only occurs significantly at lower state of charges (at 3.3 V and below) in the lower frequency range throughout the investigations (**Figure 7**, right). The electrode-resolved spectra (**Figure 8**) exhibits that the 3rd harmonic only occurs at 3.3 V at the cathode in discharge direction. Therefore, probably, the 3rd harmonic appears due to the inhibited solid-state lithium-ion diffusion within NMC (Amin and Chiang, 2016; Wiemers-Meyer et al., 2016). That the 3rd harmonic occurs as a response to diffusion processes in electrochemical systems has already been suggested in literature (Wolff et al., 2018, 2019).

When cell temperature is changed and the state of charge remains constant, the overpotentials at both electrodes increase in a similar manner with decreasing temperature. The results of NLEIS spectra compared to current-overpotential characteristics show that the occurrence of the 2nd harmonic correlates with the presence of significant overpotentials. Furthermore, the 2nd

TABLE 3 | Experimental parameters for EIS spectra, I-Pulse measurements, and NLEIS spectra as a function of state of charge.

	T	Freq	AC	DC	E _{cell}
EIS	20°C	200 kHz–5 mHz (30 freq. per decade)	2 mA	/	3.3 V
I-Pulse	20°C	/	/	±1–5 mA ΔI = 1 mA ±1–34 mA ΔI = 2 mA	2.9–4.0 V 3.3 V
NLEIS (full cell)	20°C	400–0.2 Hz (10 freq. per decade)	2 mA	±5 mA	2.9 V 3.3 V 3.7 V 4.0 V
NLEIS (electrode-resolved)	20°C	400–0.2 Hz (10 freq. per decade)	2 mA	±5 mA	3.3 V

harmonic's frequency range matches with the frequency range of the charge transfer resistance for both electrodes at lowered temperature (0°C), respectively. The occurrence of 2nd harmonic may therefore be attributed to the kinetic inhibition of the charge transfer process.

On the basis of experimental data of this work and existing results from literature, in this work suggestions on the cause of 2nd and 3rd harmonic within a lithium-ion battery were made. However, further experiments have to be carried out in order to be able to make educated proposals. One approach would be to investigate other cell systems by varying the electrode materials.

EXPERIMENTAL

The investigated system is a lithium-ion battery in a three-electrode setup (EL-Cell, Germany), of which the anode and cathode represent round die-cuts (diameter = 18 mm, electrode surface ~2.55 cm²). A metallic lithium reference ring is implemented in the separator. The corresponding electrode components are listed in the **Tables 1–3**.

EIS, NLEIS, and Current-Pulse Measurements

All data in this manuscript are based on a minimum of four cell replicates.

EIS and I-Pulse measurements were performed with a VMP3-Potentiostat (Biologic, France). The NLEIS was carried out by means of a VMP3 Potentiostat (BioLogic, France) which was solely used to generate the analog input signal (DC+AC). A DAQ-device (NI 9251, National Instruments, Germany) was connected to the E-Monitor of the VMP3-Potentiostat to record the analog output signal of the lithium-ion battery. This setup was chosen, since we required the raw data of the output signal and not the processed one. All temperature measurements (in the range between 0 to 20°C) were carried out in a climate chamber (MK58, Binder, Germany). EIS and I-Pulse measurements were recorded in three-electrode setup. The NLEIS spectra were

recorded in a complete cell arrangement and a three-electrode setup was used for selected measurement parameters only, as the electron—resolved spectra in this setup are still laborious at this time.

DATA AVAILABILITY STATEMENT

All datasets generated for this study are included in the article/Supplementary Material.

AUTHOR CONTRIBUTIONS

All authors listed have made a substantial, direct and intellectual contribution to the work, and approved it for publication.

REFERENCES

- Ahlgren, P., Jarneving, B., and Rousseau, R. (2003). Requirements for a cocitation similarity measure, with special reference to Pearson's correlation coefficient. *J. Am. Soc. Inf. Sci. Technol.* 54, 550–560. doi: 10.1002/asi.10242
- Amin, R., and Chiang, M. (2016). Characterization of electronic and ionic transport in Li_{1-x}Ni_{0.33}Mn_{0.33}Co_{0.33}O₂ (NMC333) and Li_{1-x}Ni_{0.50}Mn_{0.20}Co_{0.30}O₂ (NMC523) as a function of Li CONTENT. *J. Electrochem. Soc.* 163, A1512–A1517. doi: 10.1149/2.0131608jes
- André, D., Meiler, M., Steiner, K., Wimmer, C. H., Soczka-Guth, T., and Sauer, D. U. (2011). Characterization of high-power lithium-ion batteries by electrochemical impedance spectroscopy. I. Experimental investigation. *J. Power Sources* 196, 5334–5341. doi: 10.1016/j.jpowsour.2010.12.102
- Atebamba, J. M., Moskon, J., Pejovnik, S., and Gaberscek, M. (2010). On the interpretation of measured impedance spectra of insertion cathodes for lithium-ion batteries. *J. Electrochem. Soc.* 157:A1218. doi: 10.1149/1.3489353
- Aurbach, D. (2000). Review of selected electrode-solution interactions which determine the performance of Li and Li ion batteries. *J. Power Sources* 89, 206–218. doi: 10.1016/S0378-7753(00)00431-6
- Bard, A. J., and Faulkner, L. R. (2001). *Electrochemical Methods*. New York, NY: Wiley.
- Bugga, R. V., and Smart, M. C. (2010). Lithium plating behavior in lithium-ion cells. *ECS Trans.* 25, 241–252. doi: 10.1149/1.3393860
- Cañas, N. A., Hirose, K., Wagner, N., and Friedrich, K. A. (2013). Investigations of lithium-sulfur batteries using electrochemical impedance spectroscopy. *Electrochim. Acta* 97, 42–51. doi: 10.1016/j.electacta.2013.02.101
- Caverly, R. H., and Hiller, G. (1987). Distortion in P-I-N diode control circuits. *IEEE Trans. Microw. Theory Tech.* 35, 492–501. doi: 10.1109/TMTT.1987.1133689
- Farmann, A., Waag, W., and Sauer, D. U. (2016). Application-specific electrical characterization of high power batteries with lithium titanate anodes for electric vehicles. *Energy* 112, 294–306. doi: 10.1016/j.energy.2016.06.088
- Gordon, I. A. J., Grugeon, S., Takenouti, H., Tribollet, B., Armand, M., Davoisne, C., et al. (2017). Electrochemical impedance spectroscopy response study of a commercial graphite-based negative electrode for Li-ion batteries as function of the cell state of charge and ageing. *Electrochim. Acta* 223, 63–73. doi: 10.1016/j.electacta.2016.12.013
- Harting, N., Wolff, N., Röder, F., and Krewer, U. (2017). Nonlinear frequency response analysis (NFRA) of lithium-ion batteries. *Electrochim. Acta* 248, 133–139. doi: 10.1016/j.electacta.2017.04.037
- Heins, T. P., Schlüter, N., and Schröder, U. (2017). Electrode-resolved monitoring of the ageing of large-scale lithium-ion cells by using electrochemical impedance spectroscopy. *Chem. Electro. Chem.* 4, 2921–2927. doi: 10.1002/celec.201700686
- Huang, J., Li, Z., and Zhang, J. (2015). Dynamic electrochemical impedance spectroscopy reconstructed from continuous impedance measurement of single frequency during charging/discharging. *J. Power Sources* 273, 1098–1102. doi: 10.1016/j.jpowsour.2014.07.067
- Illig, J., Inder, M., Chrobak, T., Schmidt, J. P., Klotz, D., and Ivers-Tiffée, E. (2012). Separation of charge transfer and contact resistance in LiFePO₄-cathodes by impedance modeling. *J. Electrochem. Soc.* 159, A952–A960. doi: 10.1149/2.030207jes
- Jossen, A. (2006). Fundamentals of battery dynamics. *J. Power Sources* 154, 530–538. doi: 10.1016/j.jpowsour.2005.10.041
- Kiel, M., Bohlen, O., and Sauer, D. U. (2008). Harmonic analysis for identification of nonlinearities in impedance spectroscopy. *Electrochim. Acta* 53, 7367–7374. doi: 10.1016/j.electacta.2008.01.089
- Latz, A., and Zausch, J. (2013). Thermodynamic derivation of a Butler-Volmer model for intercalation in Li-ion batteries. *Electrochim. Acta* 110, 358–362. doi: 10.1016/j.electacta.2013.06.043
- Mao, Q., Krewer, U., and Hanke-Rauschenbach, R. (2010). Total harmonic distortion analysis for direct methanol fuel cell anode. *Electrochem. Commun.* 12, 1517–1519. doi: 10.1016/j.elecom.2010.08.022
- Murbach, M. D., Hu, V. W., and Schwartz, D. T. (2018). Nonlinear electrochemical impedance spectroscopy of lithium-ion batteries: experimental approach, analysis, and initial findings. *J. Electrochem. Soc.* 165, A2758–A2765. doi: 10.1149/2.071181jes
- Park, M., Zhang, X., Chung, M., Less, G. B., and Sastry, A. M. A. (2010). Review of conduction phenomena in Li-ion batteries. *J. Power Sources* 195, 7904–7929. doi: 10.1016/j.jpowsour.2010.06.060
- Sacci, R. L., Seland, F., and Harrington, D. A. (2014). Dynamic electrochemical impedance spectroscopy, for electrocatalytic reactions. *Electrochim. Acta* 131, 13–19. doi: 10.1016/j.electacta.2014.02.120
- Saccoccio, M., Wan, T. H., Chen, C., and Ciucci, F. (2014). Optimal regularization in distribution of relaxation times applied to electrochemical impedance spectroscopy: ridge and lasso regression methods - a theoretical and experimental study. *Electrochim. Acta* 147, 470–482. doi: 10.1016/j.electacta.2014.09.058
- Shmilovitz, D. (2005). On the definition of total harmonic distortion and its effect on measurement interpretation. *IEEE Trans. Power Deliv.* 20, 526–528. doi: 10.1109/TPWRD.2004.839744
- Suematsu, Y., Hong, T., Chung, S., and Kang, M. (1982). Harmonic characteristics of laser diodes. *J. Opt. Commun.* 3, 42–48. doi: 10.1515/JOC.1982.3.2.42
- Umeda, M., Dokko, K., Fujita, Y., Mohamedi, M., Uchida, S., and Selman, J. R. (2001). Electrochemical impedance study of Li-ion insertion into mesocarbon microbead single particle electrode: part I. Graphitized carbon. *Electrochim. Acta* 47, 885–890. doi: 10.1016/S0013-4686(01)00799-X
- Vetter, J., Novák, P., Wagner, M. R., Veit, C., Möller, K. C., Besenhard, J. O., et al. (2005). Ageing mechanisms in lithium-ion batteries. *J. Power Sources* 147, 269–281. doi: 10.1016/j.jpowsour.2005.01.006
- Wan, T. H., Saccoccio, M., Chen, C., and Ciucci, F. (2015). Influence of the discretization methods on the distribution of relaxation times deconvolution: implementing radial basis functions with DRTools. *Electrochim. Acta* 184, 483–499. doi: 10.1016/j.electacta.2015.09.097

ACKNOWLEDGMENTS

The authors would like to thank the Battery Lab Factory for providing the electrode materials and Bogdan Petrescu from BioLogic for the very helpful technical support. We acknowledge support by the German Research Foundation and the Open Access Publication Funds of the Technische Universität Braunschweig.

SUPPLEMENTARY MATERIAL

The Supplementary Material for this article can be found online at: <https://www.frontiersin.org/articles/10.3389/fenrg.2019.00151/full#supplementary-material>

- Way, W. I. (1987). Large signal nonlinear distortion prediction for a single-mode laser diode under microwave intensity modulation. *J. Light. Technol.* 5, 305–315. doi: 10.1109/JLT.1987.1075517
- Wiemers-Meyer, S., Kasnatscheew, J., Rodehorst, U., Streipert, B., Jakelski, R., Wagner, R., et al. (2016). Learning from overpotentials in lithium ion batteries: a case study on the LiNi 1/3 Co 1/3 Mn 1/3 O 2 (NCM) cathode. *J. Electrochem. Soc.* 163, A2943–A2950. doi: 10.1149/2.0461614jes
- Wolff, N., Harting, N., Heinrich, M., Röder, F., and Krewer, U. (2018). Nonlinear frequency response analysis on lithium-ion batteries: a model-based assessment. *Electrochim. Acta* 260, 614–622. doi: 10.1016/j.electacta.2017.12.097
- Wolff, N., Harting, N., Röder, F., Heinrich, M., and Krewer, U. (2019). Understanding nonlinearity in electrochemical systems. *Eur. Phys. J. Spec. Top.* 227, 2617–2640. doi: 10.1140/epjst/e2019-800135-2
- Wu, M. S., Chiang, P. C. J., and Lin, J. C. (2005). Electrochemical investigations on advanced lithium-ion batteries by three-electrode measurements. *J. Electrochem. Soc.* 152:A47. doi: 10.1149/1.1825385
- Wu, S. L., Zhang, W., Song, X., Shukla, A. K., Liu, G., Battaglia, V., et al. (2012). High rate capability of Li(Ni_{1/3} Mn_{1/3} Co_{1/3})O₂ electrode for Li-ion batteries. *J. Electrochem. Soc.* 159, A438–A444. doi: 10.1149/2.062204jes
- Xu, K., Von Cresce, A., and Lee, U. (2010). Differentiating contributions to “ion transfer” barrier from interphasial resistance and Li⁺ desolvation at electrolyte/graphite interface. *Langmuir* 26, 11538–11543. doi: 10.1021/la1009994
- Xu, N., and Riley, D. J. (2013). Nonlinear analysis of a classical system: the faradaic process. *Electrochim. Acta* 94, 206–213. doi: 10.1016/j.electacta.2013.01.141
- Yu, P., Popov, B., Ritter, J., and White, R. (1999). Determination of the lithium ion diffusion coefficient in graphite. *J. Electrochem. Soc.* 146, 8–14. doi: 10.1149/1.1391556
- Zabara, M. A., Uzundal, C. B., and Ulgut, B. (2019). Linear and nonlinear electrochemical impedance spectroscopy studies of Li/SOCl₂ batteries. *J. Electrochem. Soc.* 166, A811–A820. doi: 10.1149/2.1231904jes
- Zhang, J., Wu, N., Song, S., Huang, J., and Li, Z. (2014). Exploring differences between charge and discharge of LiMn₂O₄/Li half-cell with dynamic electrochemical impedance spectroscopy. *Electrochim. Acta* 131, 228–235. doi: 10.1016/j.saa.2014.01.111

Conflict of Interest: The authors declare that the research was conducted in the absence of any commercial or financial relationships that could be construed as a potential conflict of interest.

Copyright © 2019 Ernst, Heins, Schlüter and Schröder. This is an open-access article distributed under the terms of the Creative Commons Attribution License (CC BY). The use, distribution or reproduction in other forums is permitted, provided the original author(s) and the copyright owner(s) are credited and that the original publication in this journal is cited, in accordance with accepted academic practice. No use, distribution or reproduction is permitted which does not comply with these terms.